Hindawi
Advances in Civil Engineering
Volume 2021, Article ID 8824793, 14 pages
https://doi.org/10.1155/2021/8824793

Research Article

Analysis of Stress and Deformation Characteristics of Deep-Buried Phyllite Tunnel Structure under Different Cross-Section Forms and Initial Support Parameters

Hao Wu,[1,2] **Xiaohua Yang**,[1,2] **Shichun Cai**,[1] **Binjing Zhao**,[1] **and Kunlong Zheng**[1]

[1]*School of Highway, Chang'an University, Xi'an 710064, China*
[2]*Shannxi Provincial Major Laboratory for Highway Bridge&Tunnel, Xi'an 710064, China*

Correspondence should be addressed to Xiaohua Yang; xiaohuay@126.com

Received 11 August 2020; Revised 5 December 2020; Accepted 23 December 2020; Published 8 January 2021

Academic Editor: Xia Bian

Deep-buried soft rock tunnels exhibit low strength and easy deformation under the influence of high ground stress. The surrounding rock of the soft rock tunnel may undergo large deformation during the construction process, thereby causing engineering problems such as the collapse of the vault, bottom heave, and damage to the supporting structure. The Chengwu Expressway Tunnel II, considered in this study, is a phyllite tunnel, with weak surrounding rock and poor water stability. Under the original design conditions, the supporting structure exhibits stress concentration and large deformation. To address these issues, three schemes involving the use of the double-layer steel arch to support, weakening of the steel arch close to the excavation surface, and weakening of the steel arch away from the excavation surface to support were proposed. Using these schemes, the inverted radius was varied to explore its influence on different support schemes. For simulation, the values of the inverted radius selected were as follows: 1300 cm, 1000 cm, and 700 cm. The proposed support plan was simulated using FLAC3D, and the changes in the pressure between the initial support and surrounding rock, the settling of the vault, and the surrounding convergence were investigated. The numerical simulation results of monitoring the surrounding rock deformation show that the double-layer steel arch can effectively reduce the large deformation of the soft rock well. When the stiffness of one of the steel arches was weakened, the support's ability to control the deformation was weakened; however, it still showed reliable performance in controlling deformation. However, changing the radius of the invert had an insignificant effect on the deformation and force of the supporting structure.

1. Introduction

In the construction of mountain tunnels, the original rock is often weakly broken and buried deep, and the geological conditions are relatively complicated. After tunnel excavation, the deformation of the surrounding rock is large and may last for a long time, thereby continuously increasing the stress on the support structure. The stress often exceeds the carrying capacity of the surrounding rock and initial support and further causes splitting of primary lining, surrounding rock deformation intrusion into the tunnel clearance, and even collapse. These issues pose major challenges to the design and construction of soft surrounding rock tunnels.

In view of the problems in the construction of soft rock tunnels, many studies based on on-site monitoring have been carried out [1–5]. The stability of the soft rock tunnel is affected by the structure, strength, and groundwater conditions of the surrounding rock [6–8]. Adachi et al. [9] analysed the stability of rectangular tunnels under soft rock conditions. Yang et al. [10] proposed that the rheology of chlorite schist under low stress is not obvious, but under high stress, obvious deformation may occur, and a visco-elastoplastic rheological model was used to simulate the influence of rock mass rheological characteristics on the surrounding rock stress and deformation during tunnel excavation. Luo et al. [11] found that using the Singh–Mitchell model for deformation simulation can yield

reliable results with regard to the deformation monitoring of carbonaceous rock tunnels, and the model also can be used to predict the deformation of carbonaceous rock tunnels. Asghar et al. [12] discovered that, under the condition of high ground stress in field observation, the phyllite tunnel is prone to extrusion deformation, tunnel cross-sectional area reduction, bottom drum, and other problems, and they used Burger's creep model to simulate it using FLAC3D. The layered soft rock is prone to asymmetric deformation, which may adversely affect the supporting structure. Chen et al. [13] used Universal Discrete Element Code (UDEC) numerical simulation software to simulate the asymmetric deformation of the surrounding rock in the carbonaceous phyllite tunnel and found that the asymmetric deformation was caused by the coupling effect of the layered soft rock and shearing action along the foliation, and under the action of structural shear stress, the layered soft rock may exhibit asymmetric deformation and cause cracking along the secondary lining. The soft rock may produce large deformation under high ground stress and damage the supporting structure, which can pose a big challenge for the construction of soft rock tunnels.

Because a large deformation of the soft rock is harmful to the project being undertaken, several scholars have further explored the mechanism of large deformation of soft rock tunnels [14–16]. To explore the deformation mechanism of a deep-buried soft rock roadway, Sun et al. [17] adopted the most advanced state-of-the-art infrared thermometer and full-field strain measurement system in the model test. It was pointed out that the change in the surrounding rock temperature can reflect the change of the surrounding rock behaviour. A decrease in temperature indicates a decrease in stress and the generation of microcracks, whereas an increase in temperature indicates the occurrence of friction during excavation. Furthermore, to better explore the internal causes of large deformation of soft rocks, several scholars have investigated the physical and mechanical properties of rock samples. Hu et al. [18] studied the mechanical properties of phyllite under different humidity conditions. They found that, in uniaxial and triaxial compression tests, the strain of dry phyllite increased linearly with increasing stress. When the confining pressure was 10 MPa and as the immersion time increased, Poisson's ratio of the sample increased and compressive strength and elastic modulus decreased. Furthermore, the longer the water immersion time, the more obvious were the characteristics of the soft rock. Xu et al. [19] used triaxial compression tests to study the anisotropy of phyllite under different water content conditions. The microscopic damage mechanism on the fracture surface of the specimen was obtained through SEM fractographic studies and 3D laser profilometry. Additionally, they used the temporal and spatial distributions of the AE counts to analyse the initiation and propagation of microcracks.

To cope with the damage caused by the large deformation of the soft rock, several coping methods have been proposed in engineering practice and theoretical research [20–24]. Zhang et al. [25] believed that setting the reserved deformation in the tunnel support structure can effectively reduce the damage caused by the large deformation of the soft rock tunnel, and the reserved deformation should be set between the initial support and secondary lining. Moreover, it is important to select the size of the reserved deformation. If the reserved deformation is too large, the cost is high; if the reserved deformation is too small, the construction process becomes complicated. Through on-site monitoring and numerical simulation analysis, Gao et al. [26] found that the support structure of soft rock tunnels can be optimized by weakening the anchor while enhancing the initial support stiffness and strength, thereby saving costs. Sun et al. [27] studied the system of negative Poisson's ratio (NPR) constant resistance and large deformation anchor cable support. They compared the numerical simulation with the field test data and concluded that the NPR anchor support significantly reduced the asymmetric deformation of the tunnel surrounding rock, and the deformation of the surrounding rock was smaller than that of the steel arch support. Tao et al. [28] proposed an improved "NPR cable + steel arch frame + concrete" support mode. Yang et al. [29] proposed a support scheme for deep-buried soft rock roadways, namely, a new "bolt-cable-mesh-shotcrete + shell" combined support. They used the UDEC software to simulate the support scheme and obtained reliable results.

Taking Chengwu Expressway Tunnel II as the research object, a double-layer steel arch method for the initial support was proposed. Based on this method, the deformation and stress of the proposed support scheme were investigated by varying the inverted arch radius. A FLAC3D numerical simulation software was used to further simulate the proposed schemes. Additionally, the location of the measured points and data in the actual engineering were referred to ensure the accuracy of the research.

2. Project Overview

2.1. Project Description. The Chengwu Expressway Tunnel II is a key project connecting Chengxian to Wudu (as illustrated in Figure 1). It is a separate two-way and four-lane highway tunnel located at a maximum depth of 1040 m, and the length of the tunnel is 3700 m. Furthermore, the mountain terrain is significantly steep. The natural slope of the inlet is roughly 40°, while that of the exit is roughly 50°. On-site direct shear and deformation tests were performed to obtain the basic parameters of the surrounding rock. The internal friction angle of the tunnel surrounding rock is 32°, cohesive force is 0.27 MPa, and elastic modulus is 1.3 GPa. The rock stratum is oblique to bedding, as depicted in Figure 2. Under the influence of the oblique bedding, the surrounding rock exhibits bias stress that is generally consistent with the bedding direction.

The inner contour of the tunnel has a semicircle of $R = 540$ cm, sidewall has a large radius arc with $R = 840$ cm, transition arc of the sidewall and inverted arch is $R = 100$ cm, and radius of the inverted arch is $R = 1300$ cm. During the construction process, the bench method was used, and the height of the upper step was 5.4 m. The lining structure was applied with composite lining, including the initial support, waterproof board, and secondary lining. The initial support

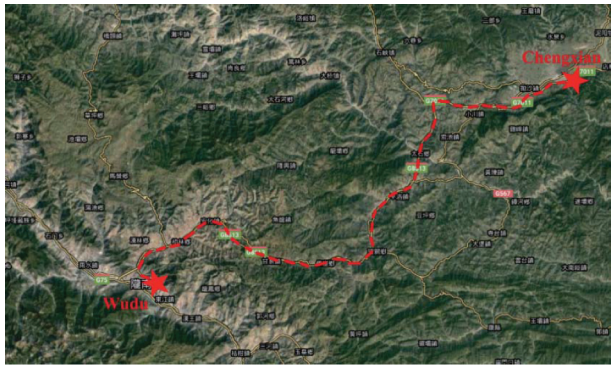

Figure 1: Project location.

Figure 2: Strata distribution of the left hole.

adopted an anchor net shotcrete and steel arch. The secondary lining was used for pouring the concrete. The C30 concrete, R27 hollow grouting anchor, and I18 steel arch were used as the initial support, and the C30 concrete was used as the secondary lining.

During the excavating process, owing to the deeper embedding, the strength of the surrounding rock mass was low and the joints were significantly developed. Additionally, the tunnel supporting structure was greatly deformed after excavation. Owing to the abovementioned reasons, collapses, such as initial lining concrete cracking, steel arch deformation, secondary lining concrete failure, inverted arch cracking, and bulging, often occurred on the work face [30]. The initial support cracking is illustrated in Figure 3.

2.2. Characteristics of the Surrounding Rock. The rock samples taken from the field site were made into slices, which were then placed under a polarizing microscope to observe the mineral composition of the rock samples [31–34]. The compositions of the rock samples are detailed in Table 1. Notably, rocks are mainly composed of sericite, chlorite, epidote, quartz, and albite. Among them, sericite and quartz have the highest proportion, accounting for 64% of the total proportion; except for the mineral components listed in Table 1, the remaining minerals account for 4% of the total proportion.

Figure 4 shows the results of the scanning electron microscope test. From the microstructure of the rock sample, it can be concluded that the schistosity plane has a

Figure 3: Detailed drawings of cracks in side walls.

Table 1: Mineral types and contents of rock samples.

Mineral type	Sericite	Chlorite	Epidote	Quartz	Albite	Remaining
Mineral content (%)	34	12	3	30	17	4

strong silky lustre. From Figure 4(a), it can be seen that the squama sericites are aligned. Furthermore, from Figure 4(b), we can observe that the clumped clusters of the chlorites are obvious. The distribution of quartz and albite in the rock is parallel to the rock's lineation, and the oriented elongated particles in the rock are formed by metamorphic recrystallization. As can be seen, the quartz particles' deformation is obvious, and the sericite intercalates between the quartz particles. Figure 4(c) shows the lineation formed by sericite and chlorite in the rock sample. It can be seen that the argillaceous components in the original rock also have different microbedding distributions. The original rock was the graphite sericite phyllite, which has undergone complex deformation and polymetamorphism. The parallel lineation foliation arrangement of graphite is depicted in Figure 4(d). Based on the microstructure and owing to the loose and directional arrangement of the rock sample structure, it can be said that its properties are extremely unstable. Macroscopically, the sample shows low rock strength, small cohesion, and high Poisson's ratio. The properties of the rock are weak with regard to the shear and tensile strength and are susceptible to external conditions.

3. Field Monitoring

3.1. Field Monitoring Plan. Considering the large deformation of the surrounding rock that occurs during tunnel excavation, a field test plan based on the tunnel was proposed. The scheme mainly included the monitoring of the stress and deformation of the tunnel support structures. In the field monitoring test, vibrating-wire pressure cells were used to test the surrounding rock pressure, and the total station was used to test the vault crown settlement and peripheral convergence displacement. The detailed arrangement of the measuring points is depicted in Figure 5. Pressure cells were arranged at the top of the arch (P1),

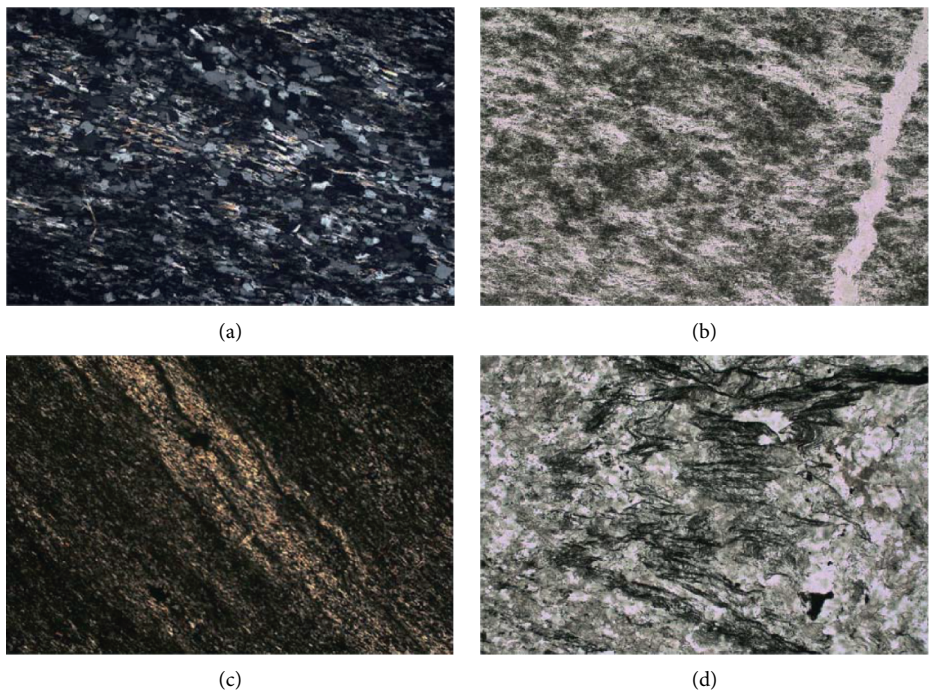

Figure 4: Microcharacteristics of rock samples.

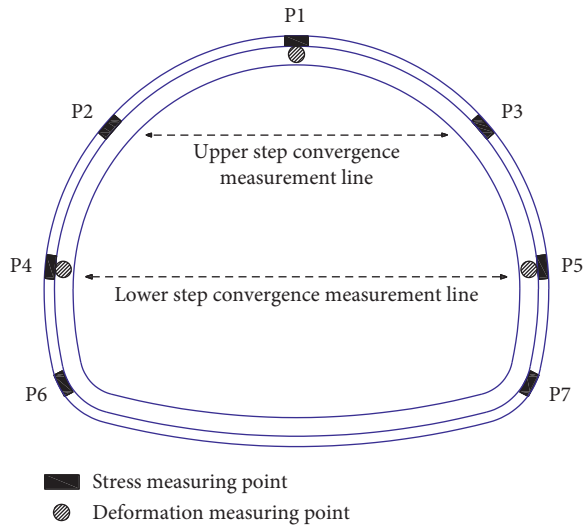

Figure 5: Arrangement of support structure stress and deformation measurement points.

excavation position of the upper (P2 and P3) and lower steps (P4 and P5), and junction of the sidewall and invert (P6 and P7). The points for measuring the peripheral convergence were arranged at positions P4 and P5.

The vibrating string pressure cell is used on-site to ensure the accuracy of the measurement data. To avoid stress concentration, when burying the pressure cell between the initial support and surrounding rock, the pressure cell should be closely attached to the back of the arch (as illustrated in Figure 6). The bottom of the cell should be flat, and there must be no gaps and unevenness between the steel arches and cell. When spraying, a space of about 20 cm between the steel arch and surrounding rock must be densely sprayed. Otherwise, the surrounding rock pressure cannot be normally transmitted to the pressure cell, thereby resulting in inaccurate test data. When burying the pressure cell between the secondary lining and initial support, the pressure cell must be fixed using steel bars and attached to the waterproof board of the initial support.

3.2. Field Monitoring Results. The stress and deformation of the supporting structure are the crucial factors affecting the stability of the surrounding rock. The ZK86 + 120 section of the left hole was selected as the monitoring section. The results of pressure between the surrounding rock and initial

(a) (b)

Figure 6: On-site measurement. (a) Installation of the pressure cell. (b) Deformation monitoring of the tunnel.

support (PSRIS) are depicted in Figure 7. The PSRIS suddenly increases around the 70th day of construction. This increase of PSRIS was caused by the lower step of excavation, and the application of locking bolts further reduced the stress. With the excavation of the lower heading of the tunnel, the cross-section showed stress concentration at the bottom of the right wall and top of the left arch, and a maximum pressure of 2.7 MPa was reached. Combined with the surrounding rock conditions of the tunnel, the rock layer was obliquely layered. Under the influence of the oblique bedding, a bias stress was generated between the surrounding rock and initial support structure, which is generally consistent with the bedding direction. This bias stress was the direct cause of the abovementioned stress concentration. In addition, the stress of the vault and left wall bottom was relatively large, i.e., close to 1 MPa. After the support was established, the stress at each measuring point gradually stabilized.

The results of the peripheral cumulative convergence (PCC) and vault cumulative subsidence (VCS) are as shown in Figure 8. It can be seen that, during the construction process, the VCS and PCC gradually stabilized, and the rate of the VCS and PCC are the same. As the tunnel face advanced, the deformation of the supporting structure exhibited a three-stage growth characteristic, and this is closely related to the excavation process: (a) rapid increase after the lower-heading excavation, (b) slow growth after the lower-heading support, and (c) even slower growth after closing the invert. This was caused by the excavation of the upper heading, following which the stress of the surrounding rock was readjusted after being disturbed. The upper-heading arch foot was directly located on the loose soft rock layer, and the overall support strength was low. After the lower-heading support, the lower steel arch is located on the precast concrete structure block and the strength of the integral support structure is strengthened; with the inverted arch closed, the initial support formed a loop, and the force was large.

The rate of the VCS was increased rapidly after excavation, and the growth rate slightly slowed down after the lower heading was supported. This trend shows that the support of the lower heading has a limited effect on the slowing of the VCS. When the inverted arch was closed, the rate of the VCS tended to slow down, indicating that the closed inverting arch has a significant effect on slowing the rate of the VCS. The rate of the PCC significantly reduced after support.

4. Numerical Simulation of Different Support Forms

4.1. Establishment of the Numerical Simulation Model. To control the supporting structure damage caused by the large deformation of the soft surrounding rock, the initial support method using a double-layer steel arch was proposed. The FLAC3D was used to simulate the soft rock tunnel under different working conditions (WCs). The numerical simulation was based on the deformation and surrounding rock parameters of the Chengwu Expressway Tunnel II. A 100 m tunnel section was selected for simulation. Additionally, to eliminate the influence of the boundary effect, the horizontal direction was taken as five times the hole diameter, and the vertical direction as three times the hole diameter. The excavation method was regarded as the core soil method, and a pregrouting advanced support method was adopted. Considering the amount of calculation required and the effectiveness of the method adopted, the rock mass in a certain range of the tunnel section was set as a layered rock mass, and a contact surface was used to simulate the joint distribution of the rock layers around the tunnel. The cable unit was used to simulate the bolt and steel tube. The initial support, secondary lining, and inverting were all simulated using solid elements and their corresponding parameters. The model is depicted in Figure 9; (a) is a cross-sectional view of the tunnel and surrounding rock and (b) is the structure of the tunnel model, which shows the inverts, lining, and upper and lower steps of the tunnel. The position of the centroid of the tunnel was used as the origin of the coordinates. The X-axis was along the horizontal direction of the tunnel, Y-axis was along the axis of tunnel, and Z-axis was along the vertical direction of the tunnel.

To monitor the vault settlement of the tunnel model and surrounding convergence, three monitoring points were set on the model section. The layout of the MPs referred to the on-site, as shown in Figure 5. The displacement of MP 1 represents the

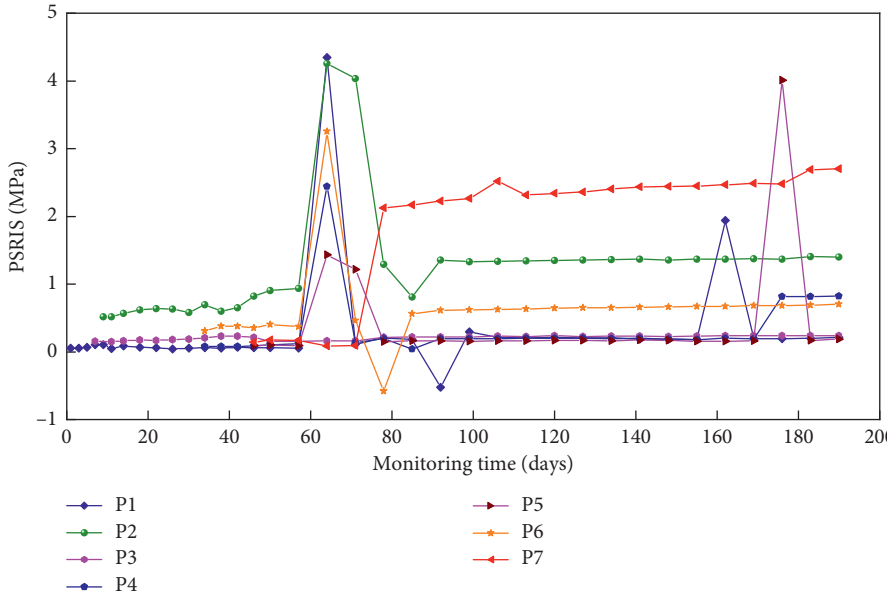

Figure 7: The results of PSRIS.

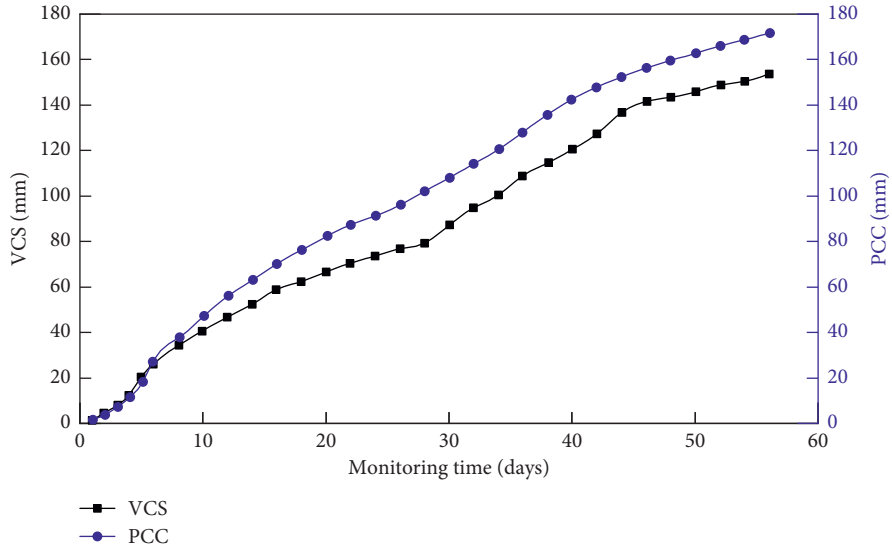

Figure 8: The results of the PCC and VCS.

settlement of the vault, and the sum of the displacements of MP 4 and MP 5 represents the convergence of the periphery.

Four WCs were simulated, which were the original support situation (WC I), double-layer steel arch support situation (WC II), weaken the steel arch close to the excavation surface (WC III), and weaken the steel arch away from the excavation surface (WC IV). Furthermore, the side near the centre of the tunnel was considered as the inside, and the side near the excavation surface as the outside, and basic parameters of the surrounding rock are listed in Table 2. Data came from field tests.

4.2. Simulation of the Original Support Situation. The support method used in the actual project was that involving the use of composite lining, which used a single-layer steel arch, and was prereinforced by the leading conduit during the excavation process. The equivalent elastic modulus of the selected steel arch was 32 GPa. The steel arch under the condition of the initial support was a single-layer steel arch corresponding to the actual project. The deformed cloud picture is depicted in Figure 10. It can be seen that, under the original supporting conditions, the deformation of the tunnel was large, the maximum settlement of the vault reached 182 mm, and the maximum floor heave of the tunnel reached 326 mm.

A monitoring point was set in the middle of the model to monitor the vault subsidence and peripheral convergence of the tunnel to compare with the actual measured on-site data during the entire excavation process. The number of steps in the simulation process was converted into the number of

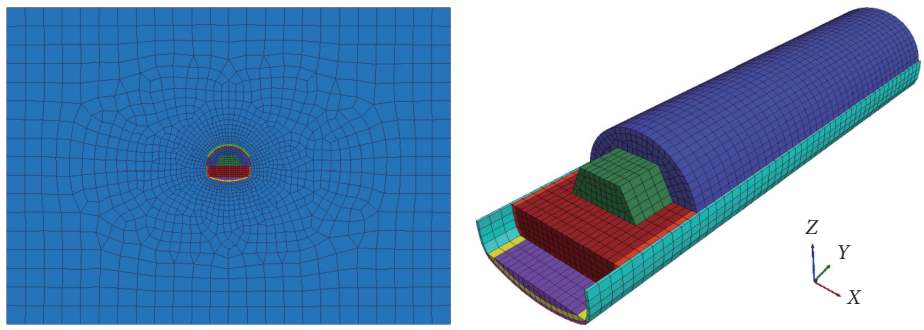

(a) (b)

Figure 9: Establishment of the tunnel model. (a) Overall view of the tunnel model. (b) Diagram of the excavation.

Table 2: Physical and mechanical parameters of the surrounding rock.

	Elastic modulus (MPa)	Density (kN/m^3)	Cohesion (MPa)	Internal friction angle (°)	Poisson's ratio
Surrounding rock	1.3×10^3	27.1	0.27	32	0.4

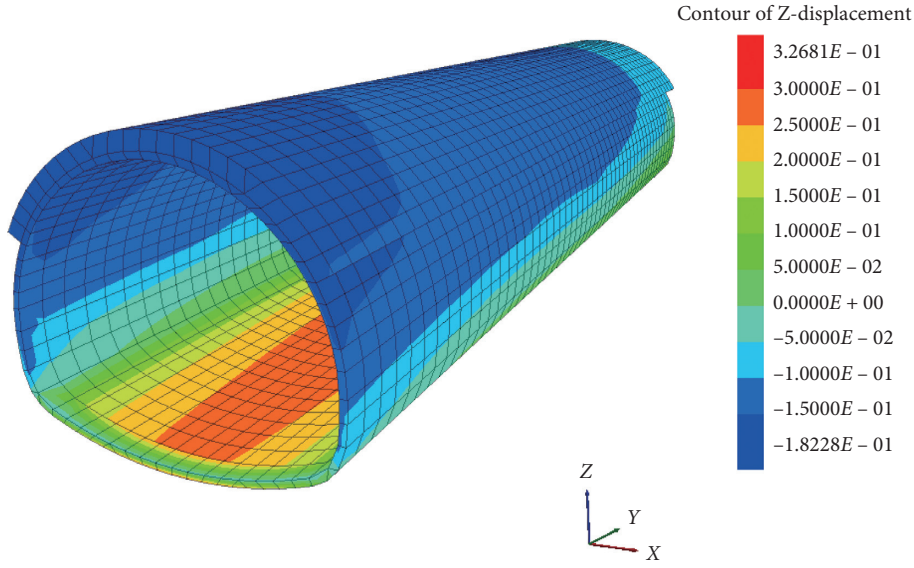

Figure 10: Deformation of the tunnel structure under the original support.

monitoring days based on the construction process, which was then compared with the in-site monitoring results, as depicted in Figure 11. Because the complex geological conditions of the surrounding rock at the site and construction speed and quality cannot be as uniform as those set in the numerical simulation, the site situation cannot be fully simulated. However, the numerical value and change trend of the VCS and PCC that can be simulated are roughly the same as on-site monitoring. The maximum difference between the actual measured value and simulated value of the vault settlement was approximately 18.6%, and the maximum difference between the two was approximately 18.2%; this proves that the simulation effect was relatively good.

The deformation of the surrounding rock was large at the beginning of excavation since the support measurement was not performed. As can be seen from Figure 11(a), the deformation of both the curves increased rapidly after excavation and levelled off after the 6th day. After the 40th day, the excavation almost had no effects on the selected section, and the settlement rate of the vault further slowed down. As the numerical simulation became relatively stable, the changes in the deformation curve also became stable. As depicted in Figure 11(b), there is an obvious inflection point on the deformation curve around the 18th day after excavation, thereby indicating that the support was beginning to function, in line with the law of large deformation of the soft rock. The deformation amount of the numerical simulation began to converge gradually after 20 days, and the deformation rate of the field monitoring results were also gradually decreasing. The final vault settlement and peripheral convergence of the numerical simulation were 132 mm and 161 mm, respectively; the final vault settlement

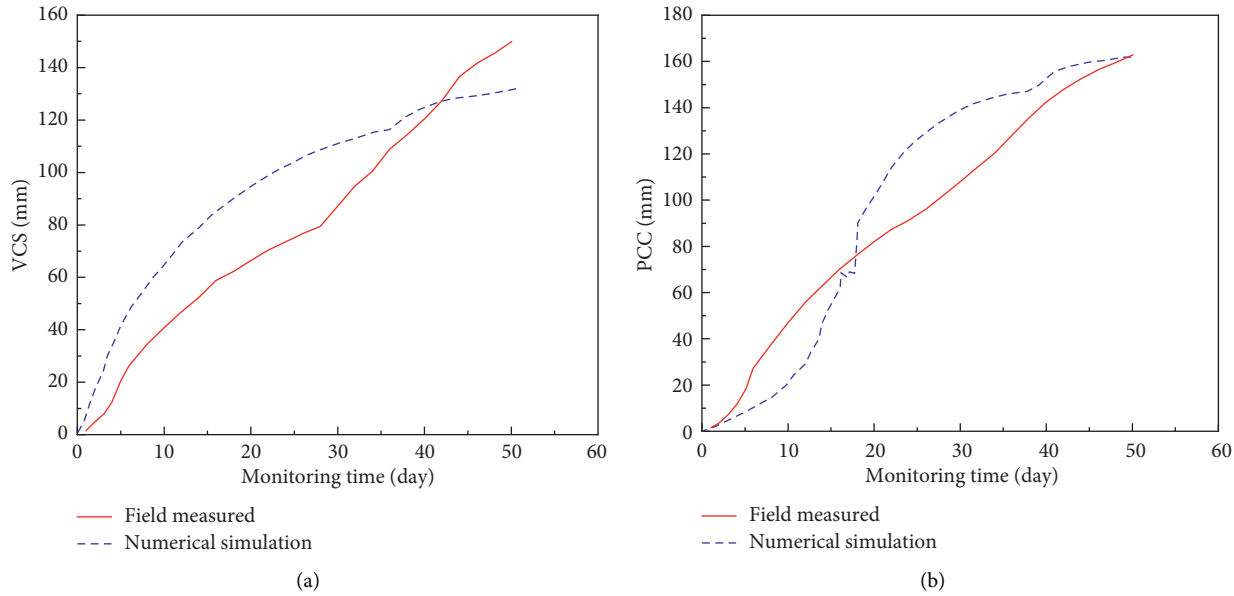

Figure 11: Comparison of numerical simulation results with in-site monitoring. (a) The VCS of the field measured and numerical simulation. (b) The PCC of the field measured and numerical simulation.

and peripheral convergence of the in-site monitoring were 149 mm and 163 mm, respectively. Based on these findings and observations, three other support schemes were simulated.

4.3. Simulation of the Double-Layer Equal Rigidity Steel Arch Support. A method involving the use of double-layer steel arches for the initial support was proposed to control the large deformation of the soft surrounding rock. A steel arch with an equivalent stiffness of 42 GPa was used for simulation. The remaining parameters and construction methods were consistent with WC I.

From Figure 12, it can be seen that the deformation trend of the tunnel model is consistent under the two WCs. The rate of vault settlement gradually decreased with time. Additionally, after the 36th day, the VCS tended to be stable. The rate of peripheral convergence continued to increase in the first 18 days and then gradually became stable. The construction of the support of the inverted arches was initiated on the 16th day. The supporting inverted arches could significantly reduce the PCC but had a negligible effect on the settlement of the VCS. After the invert support was constructed, the rate of the PCC significantly decreases. Compared with WC I, WC II could effectively control the rapid growth of the PCC produced by the single-layer steel arch support from the 18th day to the 25th day. Notably, the initial support belongs to flexible retaining, thereby allowing the surrounding rock to deform to provide a full play to the self-supporting capacity of the surrounding rock. Moreover, it can be seen from the figure that the deformation of the surrounding rock can be significantly reduced using the double-layer steel arch support. From the data, it can be concluded that, after replacing the single-layer steel arch support with the double-layer steel arch support, the final VCS decreased by 64.77% and PCC decreased by 63.93%. Furthermore, the deformation of the soft rock tunnel could be effectively reduced using the double-layer steel arch structure.

4.4. Simulation of the Variable Stiffness Double-Layer Steel Arch Support. Although the use of double-layer steel arch support can lead to a reduction in the large deformation of the soft rock tunnel, the cost involved also increased. Therefore, to weaken the strength of one of the double-layer steel arch to reduce the cost, two solutions were proposed for comparison: (a) weakening of the steel arch on the side close to the excavation face and (b) weakening of the steel arch on the side far from the excavation face. The weakening method was aimed at adjusting the equivalent elastic modulus of one layer of the two-layer steel arch to 32 GPa.

From Figure 13, it can be seen that, since only the support parameters of the steel arch were varied, the trend of the deformation curve under the three WCs is the same. We can see that the VCS curves of WC III and WC IV almost coincide, indicating that there is no obvious difference between the two WCs under the influence of the vault settlement. However, the PCC curves under these two WCs do not coincide, which indicates that when two layers of steel arches with different rigidities were used for support, it is more reasonable to place the steel arch with a lower rigidity on the outside. When a certain layer of the steel arch is weakened, the ability to control deformation may be reduced. Compared with the double-layer steel arch with equal rigidity, the PCC and VCS of WC III increased by 37.12% and 35.97%, respectively, and the PCC and VCS of WC IV increased by 37.78% and 37.98%, respectively. Furthermore, the weakening of the single-layer steel arch supported by the double-layer steel arch reduces the effect

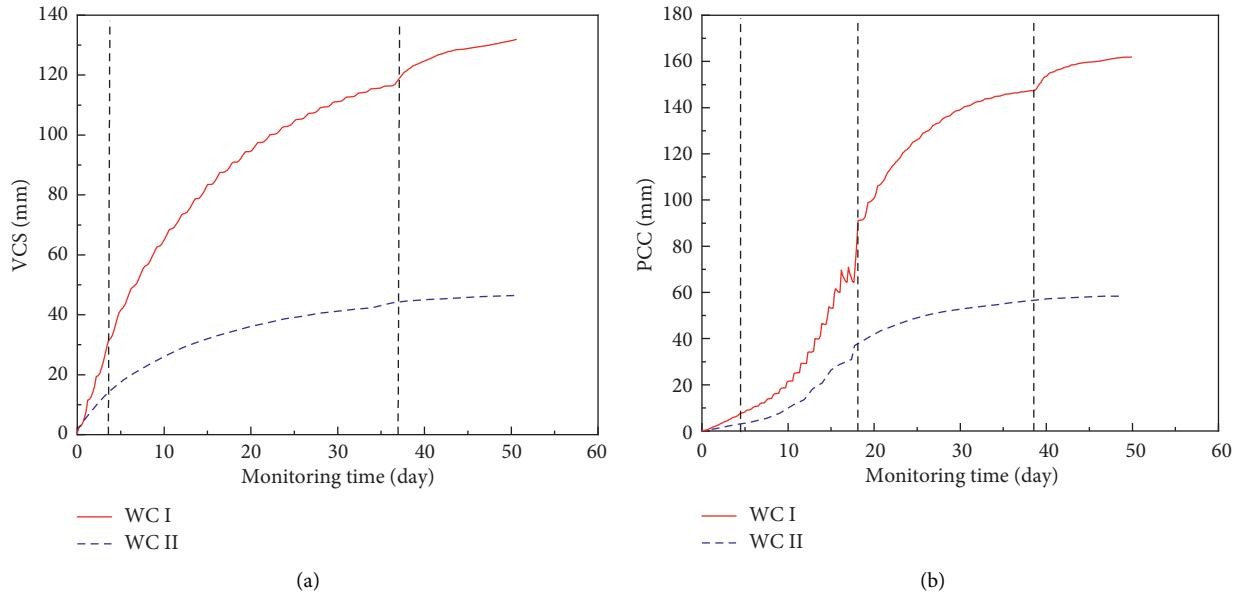

Figure 12: Comparison of single-layer steel arch support and double-layer steel arch support. (a) The VCS of WC I and WC II. (b) The PCC of WC I and WC II.

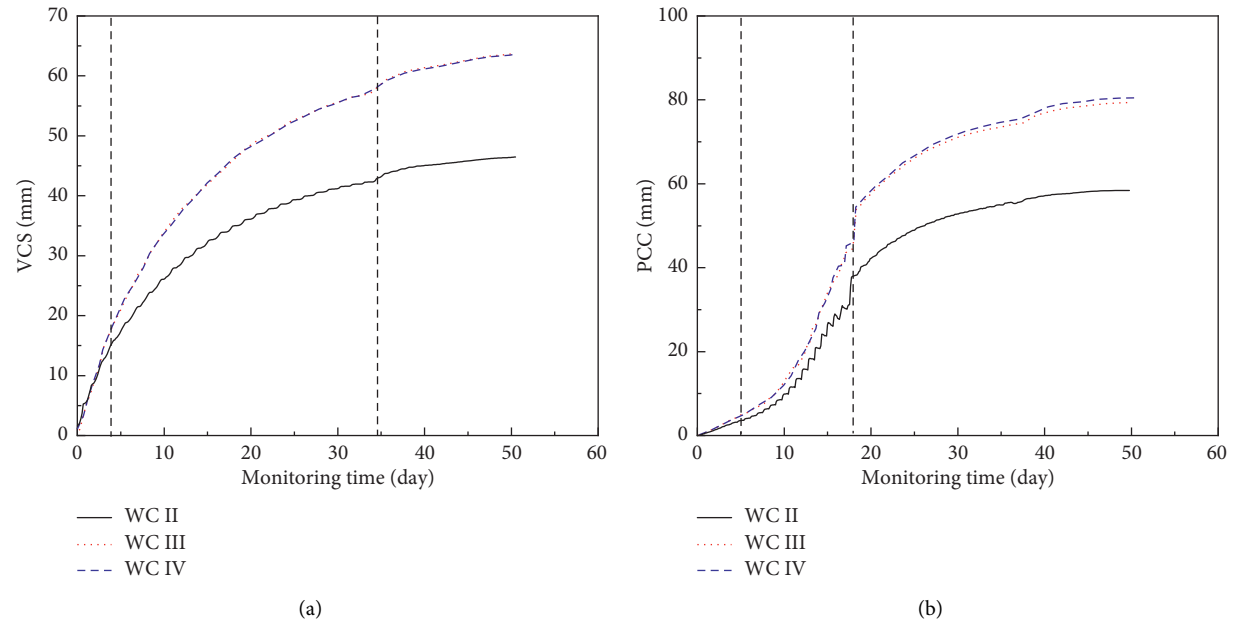

Figure 13: The effect of changing the rigidity of the steel arch on tunnel deformation. (a) The VCS of WC I, WC II, and WC IV. (b) The PCC of WC I, WC II, and WC IV.

of limiting the deformation of the tunnel. However, from the viewpoint of data, the control of tunnel deformation does not weaken significantly. Compared with the double-layer steel arch strong support, the maximum increase in deformation does not exceed 30 mm, which has a relatively insignificant effect in actual engineering practice. As can be seen from Figure 13(b), the PCC of WC III is 2.01% smaller than in the case of WC IV. Notably, when two layers of steel arches with different rigidities are used for support, it is more reasonable to place the steel arch with a lower rigidity on the outside.

5. Numerical Simulation with a Varying Arch Radius

The present section further discusses the effect of changing the arch radius on the structural deformation. Based on the discussion presented in the previous section, it can be

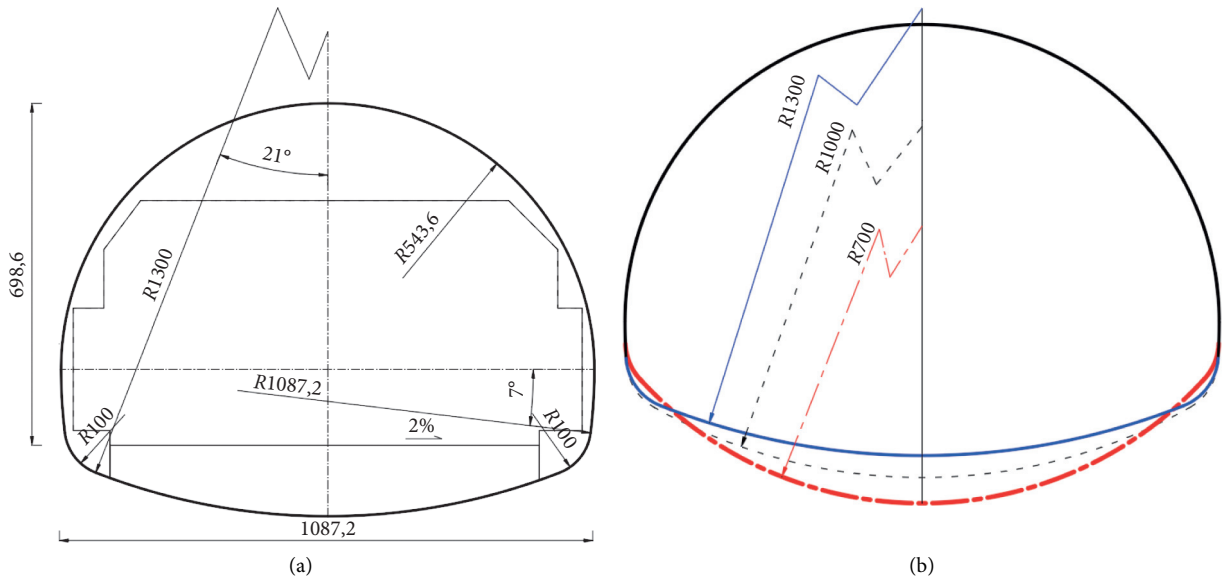

Figure 14: The tunnel outline (unit: cm). (a) The design parameters of the tunnel. (b) The tunnel outline of three radii of the invert.

concluded that the support effect of WC III is slightly better than that of WC IV, and therefore, WC IV is not discussed in the present section. To obtain more obvious results, models with 1300 cm, 1000 cm, and 700 cm inverted arch radii were simulated (as illustrated in Figure 14).

5.1. Conditions of Deformation. Considering that the stress and deformation can change with the change in the radius of the inverted arch, a technique to strengthen the rigidity of the single-layer steel arch (WC V) was proposed. Using this method, the performance of the reinforced single-layer steel arch under different arch radii can be analysed. Furthermore, WC V increases the equivalent rigidity of the steel arch from 32 GPa to 42 GPa of WC I.

Figure 15 shows the deformation after changing the radius of the invert under WC V. We can see that around the 16th day, the inverted arch began to provide the required support, and the deformation curves of the three-invert arch radius conditions began to diverge. Furthermore, only increasing the rigidity of the single-layer steel arch under the original conditions played a significant role in reducing the structural deformation. The VCS of WC V decreased from 149 mm to 85.79 mm, and the PCC of WC V decreased from 163 mm to 104.73 mm. Additionally, the VCS and PCC decreased by 42.42% and 35.75%, respectively. We can see that, in the case of a single-layer steel arch, changing the radius of the inverted arch had an insignificant effect on the deformation of the structure. The final settlement of the vault decreases with the decrease in the arch radius, and the settlements were 85.79 mm, 84.44 mm, and 83.14 mm, respectively. The change law of the PCC is consistent with that of the VCS, and the deformation amount under the three WCs reached 104.73 mm, 102.57 mm, and 95.46 mm, respectively. Additionally, when the reinforced single-layer steel arch support was used, the structural deformation decreased with the decrease of the arch radius, but the effect was not obvious.

Regarding WC II and WC III, it can be seen from Figures 16 and 17 that, by varying the radius of the inverted arch, the effect on the deformation tendency of the supporting structure was negligible. The reduction of the PCC caused by the reduction of the arch radius from 1300 cm to 1000 cm is more obvious than the reduction of the arch radius from 1000 cm to 700 cm. This shows that the change in the radius of the inverted arch has a greater effect on the peripheral convergence, and after reducing this radius to a certain extent, the gain becomes smaller. From the numerical point of view, reducing the arch radius on the basis of the original design has an insignificant effect on the deformation of the supporting structure. Under the same WC, the VCS caused by different arch radii does not exceed 3.5%, and the peripheral convergence does not exceed 6.5%. Changing the radius of the inverted arch, therefore, has a negligible effect on reducing the deformation of the supporting structure.

5.2. Conditions of Stress. As shown in Figure 5, seven MPs were selected in the numerical simulation to monitor the stress. Based on the results, the stress of the supporting structure was analysed. Because the tunnel supporting structure was mainly subjected to compressive stress, the minimum principal stress was statistically analysed. The minimum principal stress after the structure stabilized is presented in Table 3.

From Table 3, it can be seen that the internal stress of the single-layer reinforced single-layer steel arch support is exceptionally large, roughly double that of the double-layer steel arch support. Additionally, the stress conditions of WC II and WC III are similar. In WC III, only the stresses at the left and right arch feet are greater than those at WC II, and the stress at other positions is even higher than that of WC II. This finding confirmed the rationality of weakening the rigidity of the outer steel arch based on WC II.

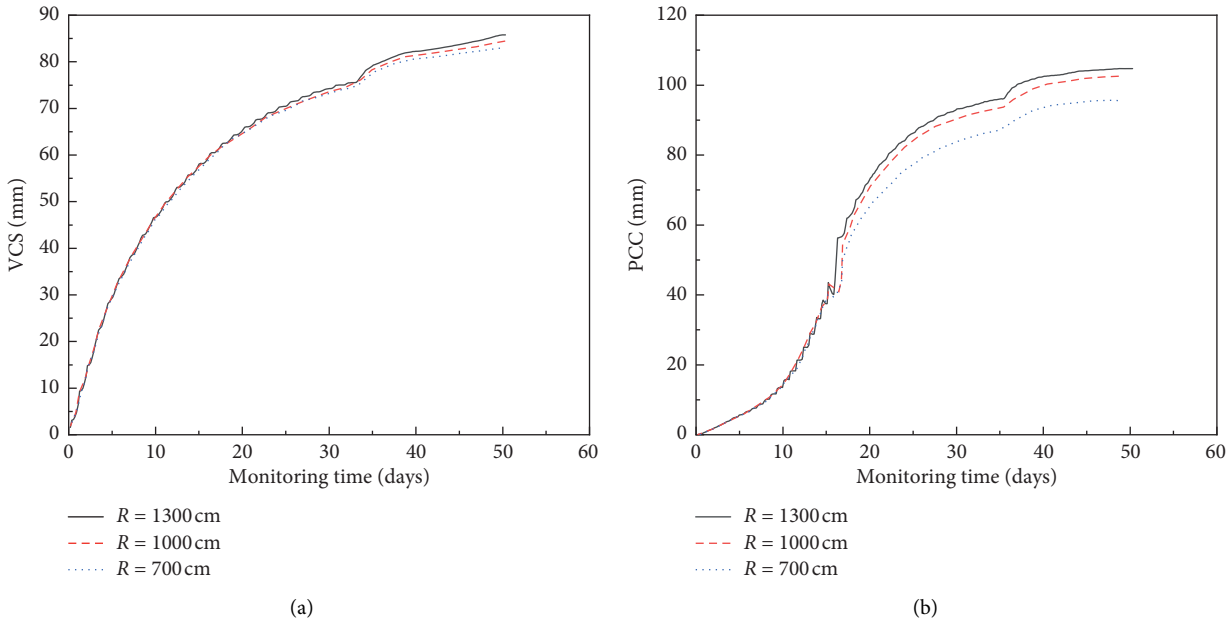

Figure 15: Deformation of the reinforced single-layer steel arch. (a) The VCS under different radii of the invert. (b) The PCC under different radii of the invert.

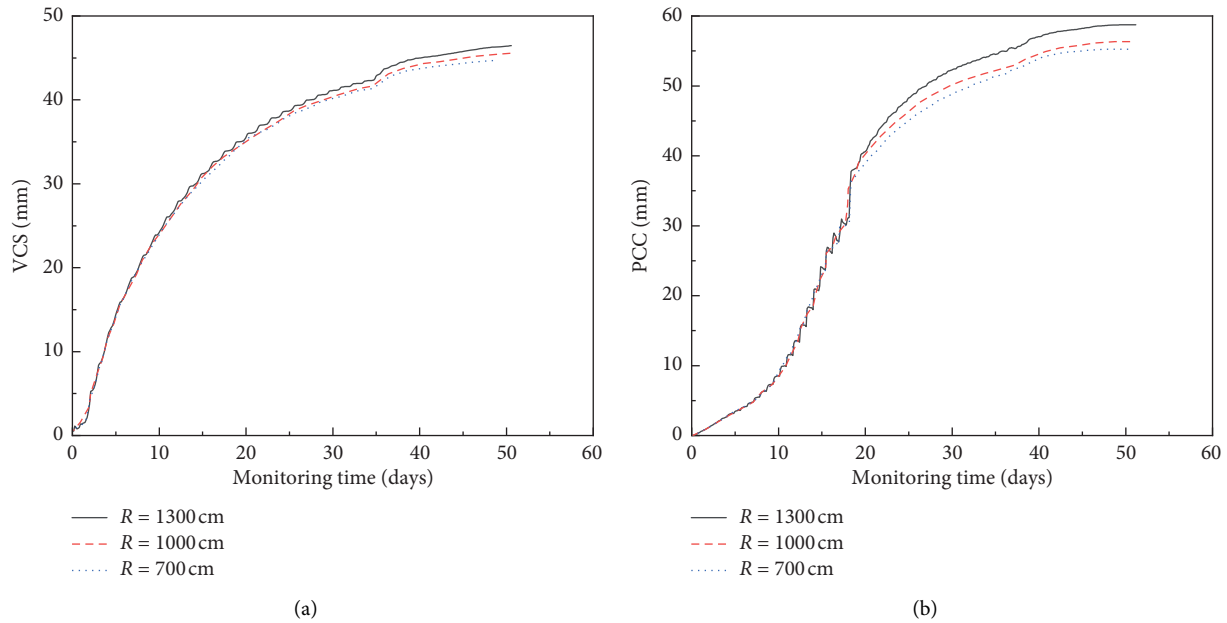

Figure 16: Deformation of the double-layer steel arch with equal rigidity. (a) The VCS under different radii of the invert. (b) The PCC under different radii of the invert.

Furthermore, by varying the radius of the inverted arch, the following observations were made: (a) there is no obvious rule for the change in the stress of WC; furthermore, the stress at the left and right arch feet becomes increasing when the radius of the inverted arch is decreased; (b) for WC II, the change in the radius of the inverted arch has almost no effect on the supporting structure stress; (c) for WC III, the change in the radius of the inverted arch has almost no effect on the MP 1–MP 4 positions. However, when the arch radius changed from 1300 cm to 1000 cm, the stress of the left and right arch feet was reduced by 25.6% and 24.9%, respectively, and the effect was more significant. In this process, the stress of the WC III support structure was slightly different from that of WC II. This conclusion shows that the stress of the WC III support structure can be optimized by reducing the arch radius from 1300 cm to 1000 cm.

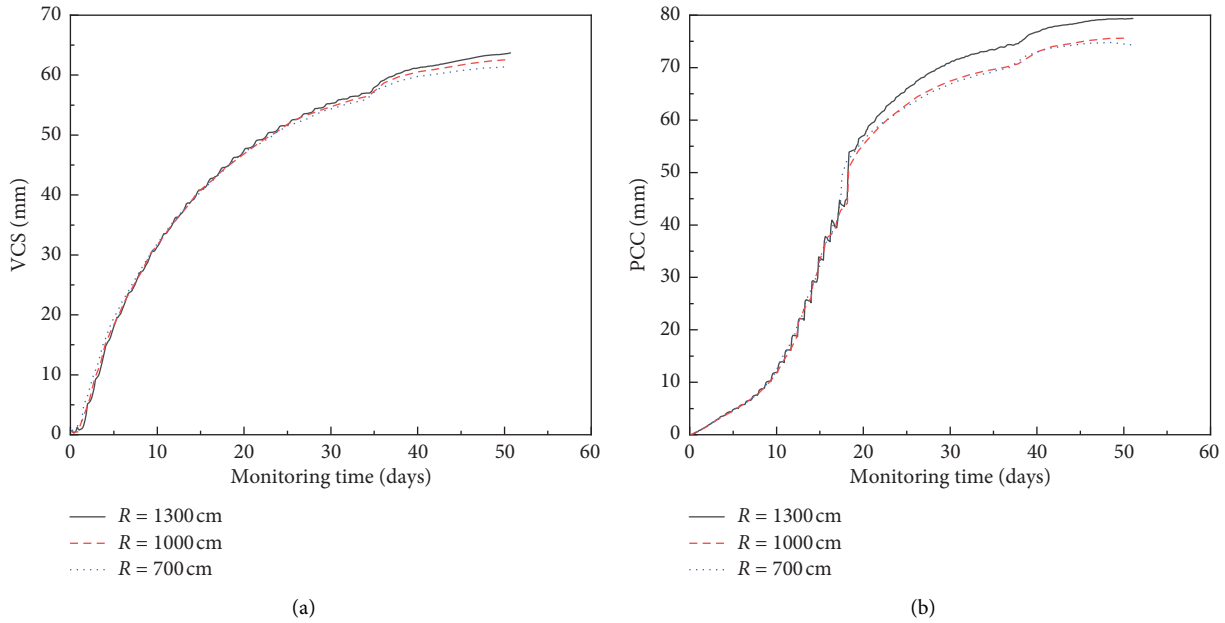

Figure 17: Deformation of the double-layer steel arch with variable stiffness. (a) The VCS under different radii of the invert. (b) The PCC under different radii of the invert.

Table 3: Stress results (unit: MPa).

WC	R (cm)	MP 1	MP 2	MP 3	MP 4	MP 5	MP 6	MP 7
WC V	1300	−1.14	−1.32	−1.26	−2.08	−2.07	−2.29	−2.29
	1000	−1.15	−1.34	−1.28	−2.07	−2.09	−2.27	−2.30
	700	−1.12	−1.31	−1.27	−2.07	−2.08	−2.37	−2.40
WC II	1300	−0.64	−0.56	−0.86	−1.16	−1.16	−1.30	−1.30
	1000	−0.65	−0.56	−0.86	−1.16	−1.16	−1.22	−1.24
	700	−0.64	−0.55	−0.86	−1.15	−1.15	−1.19	−1.20
WC III	1300	−0.56	−0.49	−0.98	−1.14	−1.15	−1.68	−1.69
	1000	−0.58	−0.47	−0.95	−1.14	−1.15	−1.25	−1.27
	700	−0.56	−0.47	−0.95	−1.14	−1.14	−1.21	−1.20

6. Conclusions

In this paper, on-site monitoring data were collected from the Chengwu Expressway Tunnel II, and indoor tests were performed using this tunnel. Furthermore, simulation was performed using FLAC3D. The present study puts forward a field-monitoring plan of using a double-layer steel arch for the initial support to address the problem of large deformation of soft rock tunnels. In the numerical simulation, the VCS and PCC of the double-layer steel arch were monitored using the proposed model. The influence of different inverted radii on different support schemes were compared and analysed. The major conclusions of this study are as follows:

(1) The results show that the deformation of the soft rock tunnel can be effectively controlled using the double-layer steel arch support. When the same rigidity steel arch support was used, the double-layer steel arch support can reduce the VCS by 64.77% and the PCC by 63.13%. Additionally, the use of a double-layer steel arch support can greatly reduce the rapid growth of surrounding rock deformation before the invert arch is closed.

(2) When two layers of steel arches with different stiffnesses are used, the ability to control deformation is weaker than that of a double-layer steel arch support. However, from the numerical point of view, two layers of steel arches with different stiffnesses also played a significant role in reducing the tunnel deformation. Compared with the double-layer steel arch with equal rigidity, the PCC and VCS of WC III increased by 37.12% and 35.97%, respectively. Additionally, the PCC and VCS of WC IV increased by 37.78% and 37.98%, respectively. When using double-layer steel arches with different rigidities, it is recommended that the steel arches with low rigidity be placed on the outside.

(3) When increasing the equivalent stiffness of the single-layer steel arch of the original support scheme from 32 GPa to 42 GPa, the VCS and PCC decreased by

42.42% and 35.75%, respectively. The reinforced single-layer steel arch support has a better effect with regard to reducing the deformation of the surrounding rock. However, the minimum principal stress was about twice that of the double-layer steel arch support.

(4) By varying the radius of the arch in the range of 700–1300 cm, it has an insignificant effect on the deformation of the proposed supporting scheme, and the difference in deformation after stabilization does not exceed 6.5%. Therefore, when using a double-layer steel arch with an equal rigidity for support, the arch radius can be increased to reduce the workload and cost. Furthermore, the reduction of the PCC caused by the reduction of the arch radius from 1300 cm to 1000 cm is more obvious as compared to the reduction of the arch radius from 1000 cm to 700 cm.

(5) By varying the radius of the invert within the range of 700–1300 cm, it had a negligible effect on the stress of the single-layer steel arch support. However, when this radius was reduced from 1300 cm to 1000 cm, the stress on the left and right arch feet of the variable stiffness double-layer steel arch support was significantly reduced. When the radius of the invert was 1000 cm and 700 cm, the minimum principal stresses of the double-layer steel arch support with equal stiffness and the double-layer steel arch support with variable stiffness were almost the same. This shows that when the radius of the invert is reduced, the stress condition of the variable stiffness double-layer steel arch can be effectively optimized.

Data Availability

All data used in this study are available from the corresponding author upon request.

Conflicts of Interest

The authors declare that there are no conflicts of interest regarding the publishing of this paper. The authors would like to declare on behalf of co-authors that the work described was original research that has not been published previously.

Authors' Contributions

All the authors listed have approved the manuscript.

Acknowledgments

This work was supported by the Natural Science Foundation of Shaanxi Province, China (Grant no. 2018JQ5001), National Natural Science Foundation of China (Grant no.51708041), Fundamental Research Funds for the Central Universities, CHD (Grant no. 300102210213), Gansu Changda Highway Co., Ltd., and Gansu Luqiao Construction Group.

References

[1] Y. Li, S. Yang, X. Tang, Y. Ding, and Q. Zhang, "Experimental investigation of the deformation and failure behavior of a tunnel excavated in mixed strata using transparent soft rock," *KSCE Journal of Civil Engineering*, vol. 24, no. 3, pp. 962–974, 2020.

[2] Y. C. Mei, W. T. Li, N. Yang, G. Wang, T. Li, and L. Sun, "Failure mechanism and optimization of arch-bolt composite support for underground mining tunnel," *Advances in Civil Engineering*, vol. 2020, Article ID 5809385, 18 pages, 2020.

[3] G. Li, F. S. Ma, J. Guo et al., "Study on deformation failure mechanism and support technology of deep soft rock roadway," *Engineering Geology*, vol. 264, Article ID 105262, 2020.

[4] Z. Chen, C. He, G. Xu, G. Ma, and W. Yang, "Supporting mechanism and mechanical behavior of a double primary support method for tunnels in broken phyllite under high geo-stress: a case study," *Bulletin of Engineering Geology and the Environment*, vol. 78, no. 7, pp. 5253–5267, 2019.

[5] G. Z. Xue, C. Gu, X. Q. Fang et al., "A case study on large deformation failure mechanism and control techniques for soft rock roadways in tectonic stress areas," *Sustainability*, vol. 11, no. 13, p. 3510, 2019.

[6] X. L. Wang, J. X. Lai, R. S. Garnes, and Y. Luo, "Support system for tunnelling in squeezing ground of Qinling-daba mountainous area: a case study from soft rock tunnels," *Advances in Civil Engineering*, vol. 2019, Article ID 8682535, 17 pages, 2019.

[7] X. Deng, J. L. Zhu, Z. H. Li et al., "Surrounding rock engineering characteristics and deformation controlling of mica schist road tunnel," *Electronic Journal of Geotechnical Engineering*, vol. 21, pp. 4587–4599, 2016.

[8] C. W. Zhang, M. Chen, G. C. Zhang et al., "Research on the failure process and stability control technology in a deep roadway: numerical simulation and field test," *Energy Science & Engineering*, vol. 8, no. 7, pp. 2297–2310, 2020.

[9] T. Adachi, F. Oka, T. Kodaka et al., "Deformation and stability analysis of rectangular tunnel in soft rock ground using a strain softening type elasto-plastic model," *Modern Tunneling Science and Technology*, vol. 1-2, pp. 533–538, 2001.

[10] F. Yang, C. Zhang, H. Zhou et al., "The long-term safety of a deeply buried soft rock tunnel lining under inside-to-outside seepage conditions," *Tunnelling and Underground Space Technology*, vol. 67, pp. 132–146, 2017.

[11] J. H. Luo, D. C. Mi, Q. Y. Ye et al., "The analysis of creep characteristics of the surrounding rock of the carbonaceous rock tunnel based on Singh-Mitchell model," *IOP Conference Series: Earth and Environmental Science*, vol. 108, no. 3, p. 032033, 2018.

[12] R. Asghar, F. Lohrasb, and D. Mohammad, "Squeezing rock conditions at phyllite-slate zone in Golab water conveyance tunnel, Iran: a case study," *Journal of Central South University*, vol. 24, no. 10, pp. 2475–2485, 2017.

[13] Z. Chen, C. He, G. Xu, G. Ma, and D. Wu, "A case study on the asymmetric deformation characteristics and mechanical behavior of deep-buried tunnel in phyllite," *Rock Mechanics and Rock Engineering*, vol. 52, no. 11, pp. 4527–4545, 2019.

[14] X. Bian, Y.-J. Cui, and X. Z. Li, "Voids effect on the swelling behaviour of compacted bentonite," *Géotechnique*, vol. 69, no. 7, pp. 593–605, 2019.

[15] X. Bian, Y.-J. Cui, L.-L. Zeng, and X.-Z. Li, "Swelling behavior of compacted bentonite with the presence of rock fracture," *Engineering Geology*, vol. 254, pp. 25–33, 2019.

[16] X. Fan, Z. J. Yang, and K. H. Li, "Effects of the lining structure on mechanical and fracturing behaviors of four-arc shaped

tunnels in a jointed rock mass under uniaxial compression," *Theoretical and Applied Fracture Mechanics*, 2021.

[17] X. Sun, F. Chen, C. Miao et al., "Physical modeling of deformation failure mechanism of surrounding rocks for the deep-buried tunnel in soft rock strata during the excavation," *Tunnelling and Underground Space Technology*, vol. 74, pp. 247–261, 2018.

[18] K. Hu, Q. Feng, and X. Wang, "Experimental research on mechanical property of phyllite tunnel surrounding rock under different moisture state," *Geotechnical and Geological Engineering*, vol. 35, no. 1, pp. 303–311, 2017.

[19] G. Xu, C. He, A. Su, and Z. Chen, "Experimental investigation of the anisotropic mechanical behavior of phyllite under triaxial compression," *International Journal of Rock Mechanics and Mining Sciences*, vol. 104, pp. 100–112, 2018.

[20] W. Liu, J. Chen, L. Chen, Y. Luo, Z. Shi, and Y. Wu, "Nonlinear deformation behaviors and a new approach for the classification and prediction of large deformation in tunnel construction stage: a case study," *European Journal of Environmental and Civil Engineering*, 2020.

[21] D. Wang, Y. J. Jiang, X. M. Sun et al., "Nonlinear large deformation mechanism and stability control of deep soft rock roadway: a case study in China," *Sustainability*, vol. 11, no. 22, p. 6243, 2019.

[22] Y. M. Zhu, L. Chen, H. Zhang et al., "Physical and mechanical characteristics of soft rock tunnel and the effect of excavation on supporting structure," *Applied Sciences-Basel*, vol. 9, no. 8, p. 1517, 2019.

[23] H. Zhang, L. Chen, Y. M. Zhu et al., "Stress field distribution and deformation law of large deformation tunnel excavation in soft rock mass," *Applied Sciences-Basel*, vol. 9, no. 5, p. 865, 2019.

[24] W. Song, H. Lai, Y. Liu, W. Yang, and Z. Zhu, "Field and laboratory study of cracking and safety of secondary lining for an existing highway tunnel in loess ground," *Tunnelling and Underground Space Technology*, vol. 88, pp. 35–46, 2019.

[25] C. L. Zhang, W. Q. Lv, L. Liu et al., "Study on the reserved deformation of large section soft rock highway tunnel based on monitoring measurement," *IOP Conference Series: Materials Science and Engineering*, vol. 452, no. 2, Article ID 022099, 2018.

[26] S.-M. Gao, J.-P. Chen, C.-Q. Zuo, W. Wang, and Y. Sun, "Structure optimization for the support system in soft rock tunnel based on numerical analysis and field monitoring," *Geotechnical and Geological Engineering*, vol. 34, no. 4, pp. 1089–1099, 2016.

[27] X. M. Sun, B. Zhang, L. Gan, Z. Tao, and C. Zhao, "Application of constant resistance and large deformation anchor cable in soft rock highway tunnel," *Advances in Civil Engineering*, vol. 2019, Article ID 4347302, 19 pages, 2019.

[28] Z. G. Tao, J. D. Cao, L. Yang et al., "Study on deformation mechanism and support measures of soft surrounding rock in Muzhailing deep tunnel," *Advances in Civil Engineering*, vol. 2020, Article ID 9367916, 14 pages, 2020.

[29] S.-Q. Yang, M. Chen, H.-W. Jing, K.-F. Chen, and B. Meng, "A case study on large deformation failure mechanism of deep soft rock roadway in Xin'an coal mine, China," *Engineering Geology*, vol. 217, pp. 89–101, 2017.

[30] J. Yu, G. Y. Liu, Y. Y. Cai et al., "Time-dependent deformation mechanism for swelling soft-rock tunnels in coal mines and its mathematical deduction," *International Journal of Geomechanics*, vol. 20, no. 3, 2020.

[31] X. H. Yang, K. L. Zheng, and L. X. Xu, "Experiment on effect of capillary crystalline material additives on cement slurry performance," *China Journal of Highway and Transport*, vol. 32, no. 7, pp. 135–157, 2019.

[32] X. Bian, Y. J. Cui, L. L. Zeng et al., "State of compacted bentonite inside a fractured granite cylinder after infiltration," *Applied Clay Science*, vol. 186, Article ID 105438, 2020.

[33] X. Fan, K. H. Li, H. P. Lai, Q. Zhao, and Z. Sun, "Experimental and numerical study of the failure behavior of intermittent rock joints subjected to direct shear load," *Advances in Civil Engineering*, vol. 2018, Article ID 4294501, 19 pages, 2018.

[34] Y. Yu, D. C. Chen, X. Q. Zhao, X. Wang, L. Zhang, and S. Zhu, "Stabilization mechanism and safety control strategy of the deep roadway with complex stress," *Advances in Civil Engineering*, vol. 2020, Article ID 8829651, 18 pages, 2020.